MASTER'S THESIS

# Master of Science in Advanced Mathematics and Mathematical Engineering

**Title:** Networks models in neuroscience: from experimental data to theoretical properties

**Author:** Guillermo Villanueva Benito

**Advisor:** Horacio G. Rotstein

**Department:** Department of Mathematics

**Academic year**: 2021-2022



UNIVERSITAT POLITÈCNICA DE CATALUNYA
BARCELONATECH
Facultat de Matemàtiques i Estadística

Universitat Politècnica de Catalunya
Facultat de Matemàtiques i Estadística

Master in Advanced Mathematics and Mathematical Engineering

Master's thesis

# Network models in neuroscience: from experimental data to theoretical properties

**Guillermo Villanueva Benito**


Supervised by Horacio G. Rotstein

Co-supervised by Farzan Nadim & Rodrigo Pena

Ponent UPC: Antoni Guillamon Grabolosa

September, 2022

I would like to thank Horacio G. Rotstein for having given me the opportunity to do interdisciplinary research at the New Jersey Institute of Technology.

I would also like to express my gratitude to Farzan Nadim and Rodrigo Pena, who have been always available for support and discussions during these months.

Last but not least, I want to thank my family, specially my parents, for their unconditional support.

## Abstract

Mathematical models are widely used to characterize the nervous system. Moreover, they continue to be the subject of further research. This work consists of two parts, where different mathematical modelling tools are exploited to solve two different problems in the field of neuroscience.

The first part is the core of this work and it is related with a recent discovered pathway from the cerebellum to the basal ganglia, two major structures in the brain. Although the cerebellum has been primarily studied for its role in the coordination of movement, preliminary experimental results on cerebellar inputs to midbrain dopaminergic neurons in the SNc indicate that this pathway is involved in two apparently disconnected behaviours: the control of voluntary movements and the evaluation of rewards in the process of positive reinforcement learning. However, the role of the cerebellum in the reward-based learning process in not well understood. We use experimental data of mice and computational modelling tools to examine the role of cerebellar inputs to the dopaminergic neurons in the SNc during behaviour, while mice perform a Pavlovian task. We propose a rate-based neuronal network model that incorporates the newly discovered cerebellar-to-SNc pathway as well as other local connectivities within the basal ganglia. We hypothesize that local inhibitory connectivities within the basal ganglia might play a fundamental role modulating dopaminergic activity in the SNc.

The second part is related with the intrinsic variability in neuronal activity and answers more theoretical questions by means of computational simulations. Although variability in neuronal responses has been exhaustively described, the mechanisms underlying variable responses to fluctuating spike inputs are not well understood. We use a simplified feedforward network model with short-term plasticity in order to study the response to different presynaptic inputs with different degrees of variability. We show that the input variability does alter the mean response of postsynaptic cells and characterize the relationship between input and output variability.

### Keywords

Neuronal network models, experimental data, reward-based learning, cerebellum, basal ganglia, neuronal frequency response, variability

### MSC2022

92B20

# Nomenclature

**DA:** Dapamine

**DCN-SNc:** Cerebellar output from the DCN to the SNc

**DCN:** Deep cerebellar nucleus. Output of the cerebellum

**SNc.DA:** Dopaminergic neurons in the SNc

**SNc.GABA:** GABAergic neurons in the SNc

**SNc:** Substantia nigra pars compacta

**SNr.GABA:** GABAergic neurons in the SNr

**SNr:** Subtantia nigra pars reticulata

# Contents

# 1. Thesis Overview

The thesis is divided in two parts. The first part is the most extensive part and we have divided its content into different chapters. In contrast, the second part is presented as a single chapter and its content is divided into different sections within the chapter. The thesis is organized as follows:

- **Chapter 1: Thesis overview.** It is this chapter. We describe the organization of the thesis.

  **Part I: Neural circuit underlying reward processing from the cerebellum to the basal ganglia**

  - **Chapter 2: Introduction.** We give some background about the cerebellum and basal ganglia. We also describe the experimental data and the main mathematical modelling tools used in part I.
  - **Chapter 3: A preliminary decoding model.** In this chapter, we analyze the cerebellar signal to the dopaminergic neurons in the SNc. We show that it can be decomposed into different components.
  - **Chapter 4: An adapting rate model with recurrent excitation.** In this chapter, we model the DCN as an excitatory population model with adaptation. Moreover, we fit the model parameters to experimental data. The output of the DCN to dopaminergic neurons in the SNc represents the DCN-SNc signal.
  - **Chapter 5: A feedforward and feedback inhibitory network model.** In this chapter, we build a 4-population rate-based neuronal network model with feedforward and feedback inhibition. The model incorporates the DCN modeled as in Chapter 4. We fit the model parameters to experimental data in order to match the measured activity of dopaminergic neurons in the SNc.
  - **Chapter 6: Conclusion.** It is the final chapter of part I and we summarize the work and discuss new lines of future research.

  **Part II: Frequency response of neurons to presynaptic spike trains**

  - **Chapter 7: An analysis in feedforward networks with short-term plasticity.** In this chapter, we study the steady-state response of postsynaptic cells subject to different types of presynaptic inputs. It includes as sections, a brief introduction, the methods, the implementation, the results and a final discussion where next research steps are stated.

Two appendices are also included:

- **Appendix A: Implementation.** In this first appendix, we give further details about the computational implementation of Part I.
- **Appendix B: Phase plane analysis.** In this second appendix, we give a detailed derivation of the nullclines in the phase-plane diagram shown in chapter 4.

## Part I

# Neural Circuit Underlying Reward Processing from the Cerebellum to the Basal Ganglia

**Summary:**

Midbrain dopaminergic centers are essential for the initiation of all voluntary movements and their disorder leads to debilitating motor dysfunction (e.g., Parkinson's disease). Dopamine is also essential for motivation and reward, such that all addictive drugs converge on activating the midbrain dopamine pathways. The cerebellum is a major structure in the brain that has been primarily studied for its role in the coordination of movement. Preliminary experimental results on cerebellar inputs to midbrain dopaminergic neurons of the substantia nigra compacta (SNc) indicate that this pathway in involved in two apparently disconnected behaviours: the control of voluntary movements and the evaluation of "rewards" in the process of positive reinforcement learning. However, the role of cerebellar modulation of SNc in the reward-based learning process is not well understood.

In this work, we use experimental data of mice and computational modelling tools to examine the role of cerebellar inputs to the dopaminergic neurons in the SNc during behaviour, while mice perform a Pavlovian task. We propose a rate-based neuronal network model that incorporates the newly discovered cerebellar-to-SNc pathway as well as other local connectivities within the basal ganglia. We hypothesize that local inhibitory connectivities within the basal ganglia play a fundamental role modulating dopaminergic activity in the SNc.

**Supervised by:** Horacio G. Rotstein and Farzan Nadim

# 2. Introduction

In part I, we build a rate-based neuronal network model that includes four neuronal populations within the cerebellum and the basal ganglia. Using experimental recordings on mice [23], our primary goal is to reproduce the experimental activity of some of these neuronal populations. We ask about the mechanisms and the network architecture that could reproduce experimental activity, and use mathematical modelling tools to build and analyze our network model.

In this chapter, we review two major structures in the brain: the cerebellum and the basal ganglia. In addition, we describe the experimental data and the mathematical modelling tools used in part I.

## 2.1 The cerebellum and the basal ganglia

The cerebellum in a major structure located in the back of the brain, Figure. 1. It has been primarily studied for its role in coordination of movement. Movement coordination is achieved due to the ability of the cerebellum to detect the difference, or "motor error," between an intended movement and the actual movement. Through cerebellar influence over upper motor neurons, the cerebellum is able to reduce the error producing coordinated movements [13]. Thus, cerebellar damage usually results in the inability to perform smooth or coordinated movements. Since the cerebellum uses its knowledge about the desired movement to compute the "motor error" signal, it is said that the cerebellum is involved in a type of learning called supervised sensorimotor learning [8].

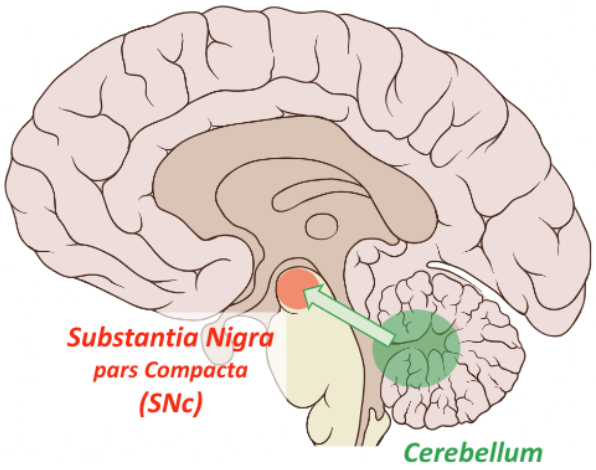


Figure 1: **Cerebellar-to-SNc pathway.** The projection from the cerebellum to the SNc directly modulates dopaminergic activity and conveys reward-value information. Author: Farzan Nadim.

Although the cerebellum has been historically associated with motor tasks, reward-based associative learning, a form of reinforcement learning, has also been recently attributed to the cerebellum [7]. In the context of reinforcement learning, behaviour is learnt through trial-and-error interactions with the environment, and decision making is done tending to maximize future rewards [12]. Therefore, these new studies suggest that the cerebellum could learn not only how to perform an action but also what actions to perform, based

on reward-base (reinforcement) learning.

Like the cerebellum, the basal ganglia influences movements primarily by modifying the activity patterns of upper motor neurons. The basal ganglia refers to a group of subcortical nuclei responsible primarily for motor control [11]. It ensures that the correct movements are initiated and maintained, while unwanted movements are suppressed [10]. Parkinson's disease is fundamentally a disorder of basal ganglia functions [2]. The basal ganglia also includes the brain's reward system, which controls motivation, incentive (desires and craving) and associative learning primarily as positive-reinforcement and classical conditioning [22].

Figure. 1 shows the substantia nigra pars compacta (SNc), which together with the substantia nigra pars reticulata (SNr) constitute the substantia nigra, a major midbrain dopaminergic nuclei within the basal ganglia that plays a fundamental role in reward and movement.

Although both the cerebellum and basal ganglia are indirect motor processing systems and both are involved in learning, these two systems have been historically studied as independent structures, mainly because no direct connection between them was reported. However, recent studies have shown that the cerebellum provides direct input to the basal ganglia dopaminergic centers, but the detailed function of these inputs or their mechanism of action remains unknown [9], [23], [1].

To sum up, both the cerebellum and the basal ganglia might be involved in reward-based associative learning, which is a form of reinforcement learning. In this work, we ask how the cerebellum and the SNc interact between them in the process of reward-based learning. In order to answer this question, we use experimental activity of neuronal population within these structures recorded during a classical conditioning or Pavlovian experiment, which is a type of reinforcement learning.

## 2.2 Experimental data

We use mice behavioral experimental data involving reward-based learning: mice were subject to a Pavlovian or classical conditioning task. In a typical Pavlovian task [18], a neutral stimulus, such as a tone, is forward paired in time with an unconditioned stimulus, such as food. Following a number of these repetitions, the stimulus comes to elicit a conditioned response (e.g. salivation), in such a way that a new association between the stimulus and the response is learnt and the neutral stimulus becomes a conditioned stimulus. We notice that reward-based learning in a typical Pavlovian task is a type of reinforcement learning. The animal learns that the cue predicts the reward and uses this information to engage itself in appropriate preparatory behaviour, such as salivation.

Our classical conditioning experiment on mice is similar to Pavlov's research work on dogs. Partially-deprived mice were given a drop of water as a reward simultaneously with a light cue [23]. Moreover, mice were trained to stop licking between 3-5 seconds prior to the cue delivery. Notice that, in this case, the conditioned stimulus is given by the light, while the conditioned response is the animal's licking. Figure. 2 shows an image of a mouse under the experiment. It also shows an schematic of the Pavlovian task that mice were subject to.

Well-trained animals were subject to three different trial cases. In the reward or regular case the unconditioned stimulus is given by a regular drop of water whereas in the higher-reward case a drop of sweet water

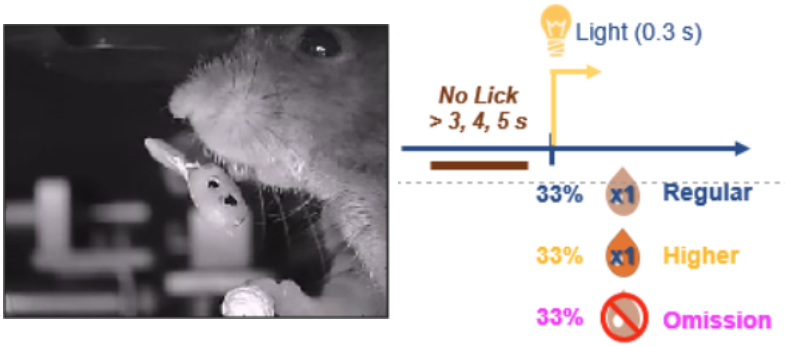


Figure 2: **Pavlovian experiment.** Left: A mouse subject to the Pavlovian task; Right: Pavlovian task schematic. Mice were trained to stop licking between 3-5 seconds prior the cue delivery. Percentages show the probabilities of a trial to be of a given type: regular (drop of water), higher (drop of sweet water) and omission (no drop of water). Source: [9].

is given to the animal. In the omission case no drop of water is given.

Data was collected during different days throughout the learning process. Different sessions were recorded within the same day, each one consisting of a fixed number of trials. A third of each session's total number of trials was of a specific trial case. In addition, data was collected from different animals and from both sides of the brain simultaneously.

Experimental data includes measured activity of the cerebellar output to the SNc (DCN-SNc) and DA neurons in the SNc (SNc.DA). Experimental data also includes the animal licking frequency during experimental tasks. Figure. 3 shows a single-session averaged signals. Although recordings from both sides of the brain are shown, only one side (left) data is used throughout part I. This is the data of interest to this project.

In [9], it is shown that the cerebellum projections to the SNc.DA neurons have two components: one that signals movement and another that is movement independent. In this project, we work under the same hypothesis and assume that the cerebellar signal does not only reflect movement, but also reward value. The input from the cerebellum, DCN-SNc signal, may contribute to the representation of reward, reflected in the activity of the SNc.DA neurons.

## 2.3 Mathematical Modelling

### 2.3.1 Rate-based models

Despite the fact that one can simulate neural network by synaptically connecting model spiking neurons, such as conductance based models, in this part we use simplified models known as rate-based models, where rather than track the spiking of every neuron, they track the averaged behavior of the spike rates of groups of neurons within a given circuit [3], [6].

In rate-based models, populations of neurons are described in terms of their firing rates. As a first step it is

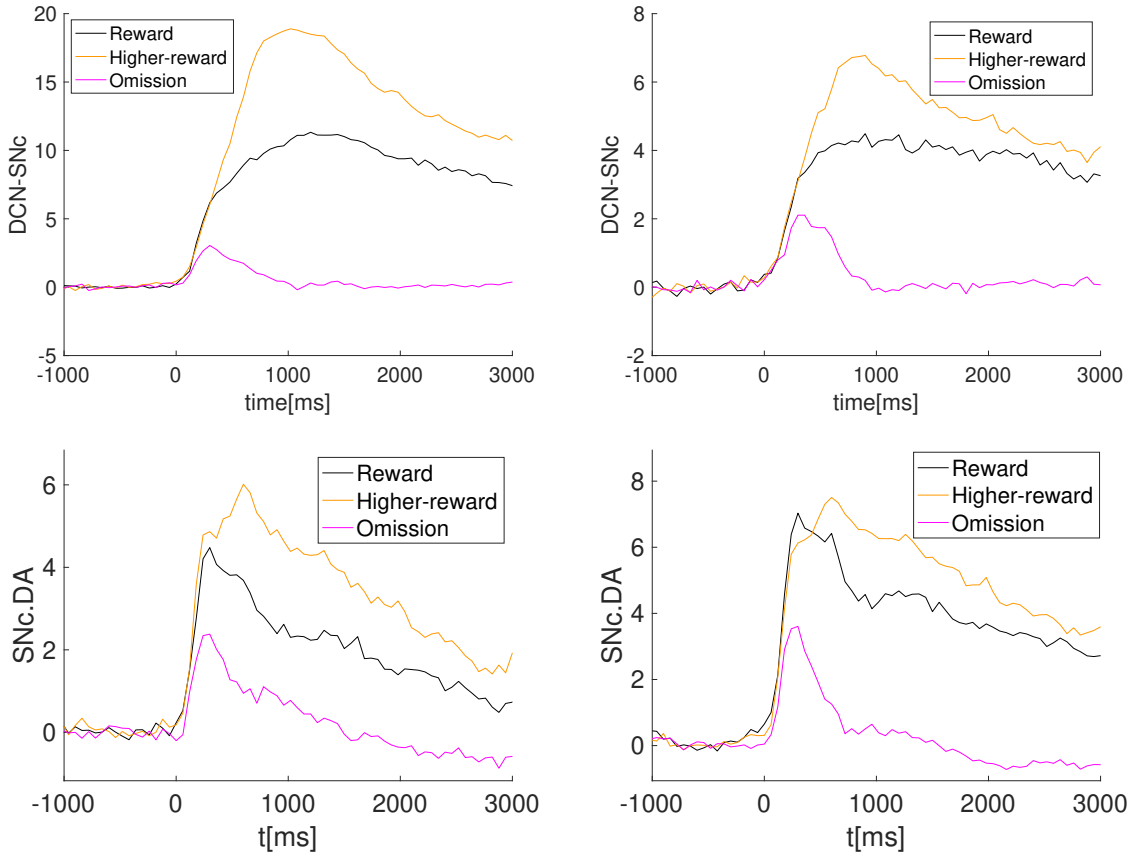


Figure 3: **Experimental data.** Average across trials within the same session. Left: one side of the brain; Right: other side of the brain; Top: DCN activity (cerebellar projections to the SNc, DCN-SNc); Bottom: dopaminergic activity in the SNc (SNc.DA). Each color represents a given trial type, namely, reward, higher-reward or omission. Number of trials: 254. The reward component cerebellar projections to SNc.DA neurons (Top) appears to be larger when the animal receives a higher-reward and small or non-existent when reward is omitted. Data: *JYK094_11RandomReward_03*

assumed that neurons under a given stimulus can be characterized by a list of times when action potentials occur. Because the sequence of action potentials generated by a given stimulus varies from trial to trial, it is used the firing rate, $r(t)$, a measure of the number of spikes over short time intervals averaged over multiple trials.

The firing rate is governed by a differential equations of general form

$$\tau \frac{dr(t)}{t} = -r(t) + F(I) \tag{1}$$

where $F$ is known as the activation function and $I$ represents external inputs.

Although, its apparent simplicity, rate-based neuronal population can be interconnected to form complex networks. In this case, $I$ also represents inputs from other population of neurons. These inputs are modeled as a proportional term to the firing rate of the neuronal populations that is connected. In chapter 5, we build

a 4-population rate-based network model involving feedforward and recurrent connectivity. The model can be viewed as a two layer (feedforward) network model, where element in the second layer are interconnected (recurrent connectivity). The DCN acts as the input layer, while nuclei within the basal ganglia constitute the output layer. Different excitatory and inhibitory connectivities interconnect these nuclei.

### 2.3.2 Adaptation

Many real neurons exhibit spike-rate adaptation. That is, when a neuron is subject to a constant stimulus (current), it is observed that interspike intervals lengthen over time before reaching its steady state value. This phenomenon is commonly modeled as an additional current in conductance-based models. We refer to the reader to [3] for more details about the adapting current.

Spike-rate adaptation can also be included into rate-based models in order to build more realistic architectures. Adaptation can be introduced as an activity dependent negative feedback [6]. In chapter 4 we build a rate-based model with adaptation.

# 3. A preliminary decoding model

In this chapter, we analyze the signal from cerebellum to the dopaminergic neuron is the SNc (DCN-SNc signal). This signal is thought to convey not only movement but also reward-value information. We decompose the whole signal into three components, namely motor-movement, cue-related, and reward value (or higher-reward-value) components. Our goal is to estimate the different types of information sent to the dopaminergic neurons in the SNc. In this chapter, we only consider the averaged DCN-SNc signal over trials.

## 3.1 Methods

Our data-decoding task consists in fitting a non-linear parametric modeling. We have used the MATLAB non-linear least squares algorithm in order to fit the model. See Appendix A for more details about the implementation.

Except for the cue-related component, we assume that each lick contributes to each component with a certain function (kernel) which belong to the parametric alpha-function space, see below. For the cue-related signal we assume that it itself belongs to the parametric alpha-function space. The estimated component is the result of adding all kernel contributions. The model is given by,

$$z_{DCN-SNc}(t) = \sum_{i=1}^{n_L} K_{mot}(t - t_i) + K_{cue}(t) + \sum_{j=1}^{n_L^k} K_{rew/hrew}(t - t_j) \tag{2}$$

where $z_{DCN}(t)$ represents averaged signal activity (z-scored), $K_{mot}$ the motor kernel associated with a lick, $K_{cue}$ the cue kernel associated with the cue, $K_{rew/hrew}$ the reward/higher-reward kernel associated with a lick in the reward/higher-reward trial case, $n_L$ the total number of licks and $n_L^k$ the total number of the first k licks after the cue. For each lick, the motor and reward kernels are centered at the lick time, $t_i$ and $t_j$ respectively. Notice that since the the DNC-SNc signal is averaged over trials, the total number of licks is the summation of licks over trials and $n_L^k = n^\circ trials \times k$.

The motor, reward/higher-reward and cue kernels belong to the parametric alpha-function space. In the field of neuroscience, alpha functions are commonly used to model synaptic conductances [19]. We use a a 3-parameter alpha-functions space and each kernel type is of the form of

$$K_*(t) = \max\left(0, a_* \frac{t - c_*}{b_*} \exp(1 - (t - c_*)/b_*)\right), \quad * = mot, cue, rew/hrew \tag{3}$$

where parameter $a$ controls the height, parameter $b$ controls the decay raise/decay time and parameter $c$ control the onset of the signal. Figure. 4 shows a representative alpha-function as a function of time.

In the following, we will summarize how we have proceed in order to estimate the different kernels and components for each trial case.

As a first step, we use available random single lick data in order to compute the motor kernel for each trial

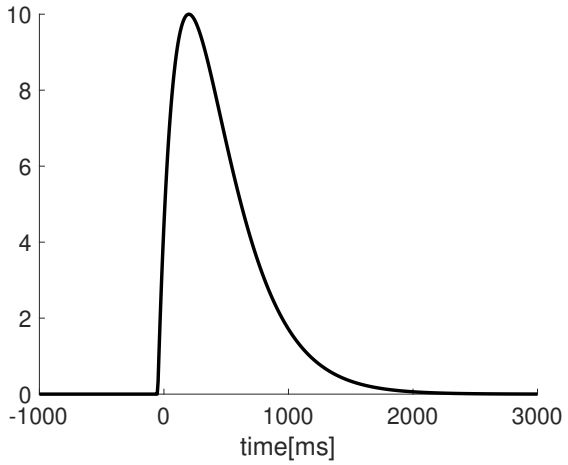


Figure 4: **Representative alpha-function.** Alpha-functions belong to the parametric alpha-function space, a 3-parameter space function. Parameter values: $a = 1$, $b = 250$ and $c = -50$.

case. These signals (not shown) correspond to spontaneous lick recordings that are not associated with the cue nor the reward. The motor-movement component for each trial case, is obtained by convolving the motor kernel with the recorded lick times for that trial case. Note that the motor-movement component is given by the first term in Eq. 2.

Secondly, we compute the cue-related component, i.e., the cue kernel. We assume that is the same for all trail cases and that it can be estimated as the difference between the signal corresponding to the omission trial case and the motor-movement component for the omission case. Notice that we are assuming that the omission signal does not have a reward-value component.

Finally, the reward-value and higher-reward-value components are obtained for the reward and higher-reward trial cases, respectively. For the reward case, we use the difference between the reward signal and the sum of the motor and cue components for the reward trial case in order to compute the reward kernel. It is obtained as the kernel function that convolved the first k lick times produces the best fit to the difference signal previously mentioned. Similarly, for the higher-reward-value component, but considering the higher-reward instead of the reward signal.

## 3.2 Results

Figure. 5-(top-left) shows the motor-movement component estimates for each trial case. Figure. 5-(top-right) shows the cue-related component added to the motor-movement component for each trial case. Notice that the omission signal is already estimated.

Finally, Figure. 5-(bottom) shows the final estimates for for each trial case. There are three plots that from left to right correspond to the results when only the first, first two or first three licks after the cue are taken into account to compute the reward or higher-reward-value components. Notice that graphically, the two-lick case produces a better estimate.

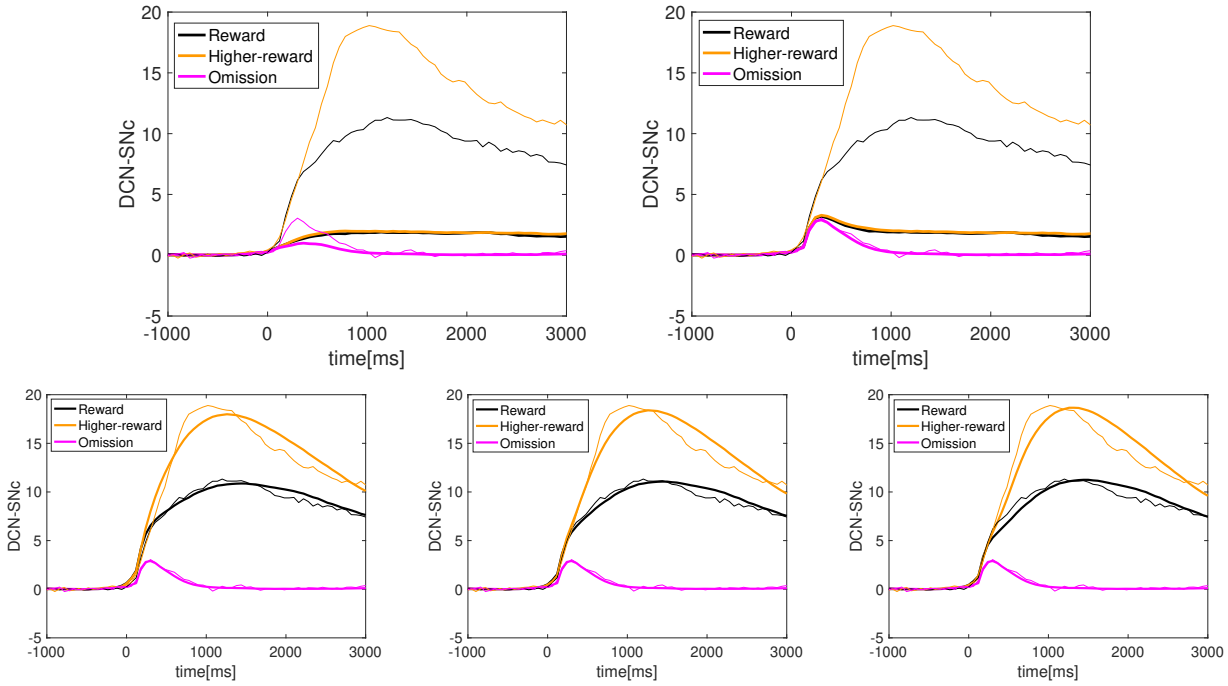


Figure 5: **Decoding model.** Component estimates of averaged DCN-SNc signal. Top left: Motor component for each trial case; Top right: Cue component added to the motor component for each trial case; Bottom: Final estimates. All components are added for each trial case. From left to right only the first, first two or first three licks after the cue have been used in order to compute the reward/higher reward components respectively.

In addition, Figure. 6 show the different obtained kernels. Notice that the reward and higher reward kernels are smaller (they have been multiplied by a factor x10) and longer signals, compared with the motor and cue kernels. They are aligned at zero, which corresponds to a lick time for motor, reward and higher reward kernels or the cue time for the cue kernel.

## 3.3 Discussion

By separating the cerebellar signal into components, we can estimate the different information send to the dopaminergic neurons. This approach enables us to quantify how each component contributes to the whole signal for each trial case. We notice that the model has been built under several assumptions and that different assumption could be tested.

On the one hand, we have assumed that the omission signal does not have a reward-value component. Although this assumption seems reasonable since no reward is given to the animal in this case, we notice that there could bea negative reward component, that is a negative signal modelling disappointing due to the lack of reward (note that the animal has already learnt the experiment).

On the other hand, we are also forcing the model to find a cue-related component. Since the cue and re-

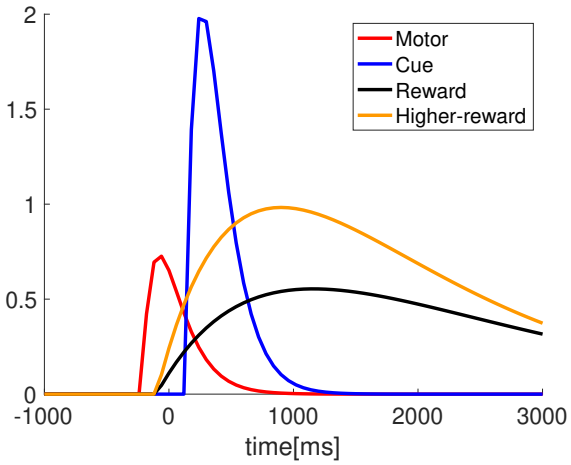


Figure 6: **Kernel functions obtained.** The decoding model estimates the different components computing their associated kernels. The reward and higher-reward kernels have been scaled (x10).

ward are simultaneously delivered, it seems reasonable to consider that there might not be be a cue-related component.

# 4. An adapting rate model with recurrent excitation

In this chapter, we model the DCN (the output of the cerebellum) as a neuronal population with recurrent excitation and adaptive feedback. The DCN, as modeled in this section, will constitute the input layer for the neuronal network model presented in the next section.

## 4.1 Methods

DCN activity is described in terms of the mean firing rate, $r_{1e}(t)$, subject to adaptation, $a(t)$

$$\tau_{1e}\frac{dr_{1e}}{dt} = -r_{1e} + \text{relumax}(J_{1e,1e}r_{1e} - J_{1e,a}a + I_{cue} + I_{rew} + I_{hrew}; m_{1e}, k_{1e}) \tag{4}$$

$$\tau_{a}\frac{da}{dt} = -a + \text{relumax}(J_{a,1e}r_{1e}; m_{a}, k_{a}) \tag{5}$$

Recurrent (self) excitation together with adaptation is incorporated into the model. We have found that the interaction of these two mechanism is able to produce

1. Long-lasting positive signals for the reward and higher-reward cases.
2. An increasing signal (positive slope) after reward and higher-reward inputs terminate.

The activation function is of a relumax type and it is a 2-parameter function of the form of Eq. 6. Figure. 7 shows the activation functions used for each variable in the model.

$$\text{relumax}(x; m, k) = \min\left(1, \max\left(0, \frac{1}{2} + \frac{x-m}{4k}\right)\right) \tag{6}$$

$I_{cue}$, $I_{rew}$ and $I_{hrew}$ are direct (external) inputs from sensory signals. They correspond to the cue, reward and higher-reward external inputs respectively. They are modeled as square pulses of the form

$$I_{in} = J_{in}\mathcal{H}(t - t_0^{in})\mathcal{H}(t - t_1^{in}), \quad in = cue, rew, hrew \tag{7}$$

where $J_{in}$ is the pulse height and $t_0^{in}$ and $t_1^{in}$ correspond to the start and end point of the pulse respectively. Sensory inputs vary with the trial case, whether it is omission, reward or higher-reward case. For the omission case, a positive cue signals is applied followed by a negative reward signal. For the reward case, a positive cue signal is applied followed by a positive reward signal. Finally, for the higher-reward case a positive cue signal is applied followed by a positive reward signal with higher amplitude as compared with the previous one. Figure 7 illustrates external inputs as a function of time for each trial case.

The model schematic diagram is shown in Figure. 8. We notice that the proposed model has 6 intrinsic parameters, 3 connectivity parameters and 9 input parameters, see Table. 1. Some parameter values have

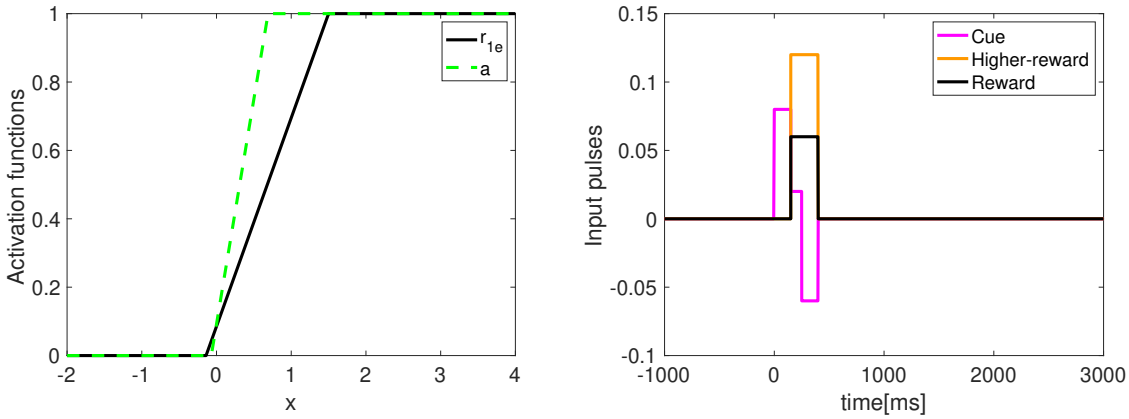


Figure 7: **Activation functions and external inputs.** Left: Activation functions used in the DCN model; Right: External input applied to the model as a functions of time for each trial case

been selected based on experimental observations whereas other parameter values has been obtained using a parameter estimation algorithm (MATLAB non-linear least squares) fitting experimental data. See more details in the Appendix A.

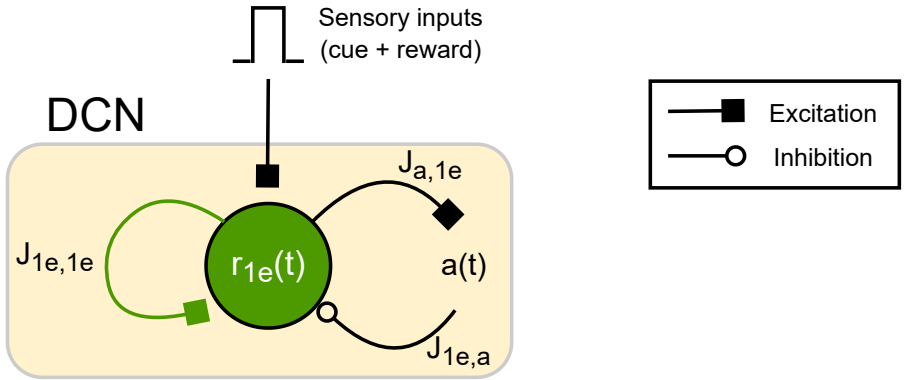


Figure 8: **DCN model schematic.** The DCN model consists in a firing-rate model with recurrent excitation ($J_{1e,1e}$) and adaptation ($J_{a,1e}$, $J_{1e,a}$).

| DCN model parameters | | |
|---|---|---|
| Intrinsic | Connectivity | Input |
| $\tau_{1e}$, $\tau_a$ | $J_{1e,1e}$ | $J_{cue}$, $J_{rew}$, $J_{hrew}$ |
| $m_{1e}$, $m_a$ | $J_{1e,a}$ | $t_0^{cue}$, $t_0^{rew}$, $t_0^{hrew}$ |
| $k_{1e}$, $k_a$ | $J_{a,1e}$ | $t_1^{cue}$, $t_1^{rew}$, $t_1^{hrew}$ |

Table 1: **DCN model parameters.** There is an overall of 18 parameters.

### 4.1.1 Phase-plane analysis

In this subsection we show the phase-plane diagram of the proposed model. We refer the reader to [20] in case of no familiarization with phase-plane analysis.

Figure. 9 shows the nullclines of the DCN model, Eqs. (4)-(5) for the case of no external sensory inputs ($I_{in} = 0, \ \ i = cue, rew, hrew$). In this case, the model has three different equilibrium points. Is is also shown the three trajectories of the three different experiments: omission, reward and higher-reward. See Appendix B for more details about how the nullclines are computed.

Sensory inputs do change the phase plane and shape trajectories. Figure. 9 also shows the nullclines of the model when there are external applied inputs. In this case, the model only presents one equilibrium point. We notice that this phase plane is temporary since external inputs are only applied at the beginning of the experiments.

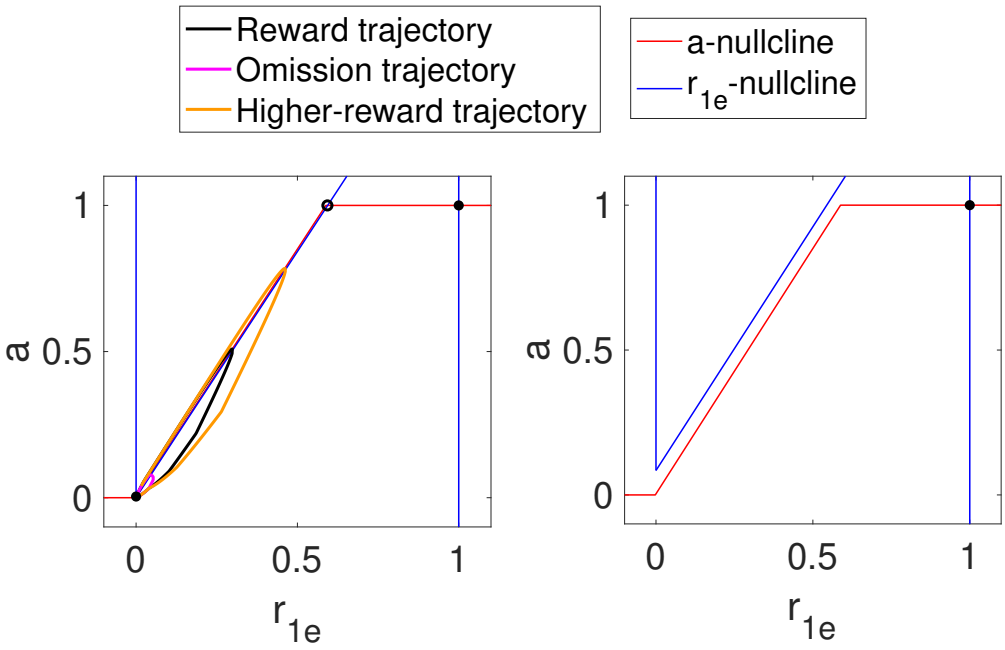


Figure 9: **DCN model phase-plane diagram.** Left: No external inputs. The model shows 3 equilibrium points (marked with black dot), two stable (left and right) and one unstable (middle); Right: External inputs injected. The model shows only one stable equilibrium point. The first sensory input applied, the cue signal, is enough to undergo the bifurcation.

From the phase plane analysis, we conclude that external inputs change the phase-plane diagram and that the model undergoes a bifurcation when external inputs are applied. This phenomenon shapes the different trajectories producing an output fitting resembling experimental data.

## 4.2 Results

The set of parameter values used, as well as a brief description of how they have been obtained, is found in Table. 3. Figure. 10 shows both the model output and experimental data for each of the three trial cases that mice were subject to.

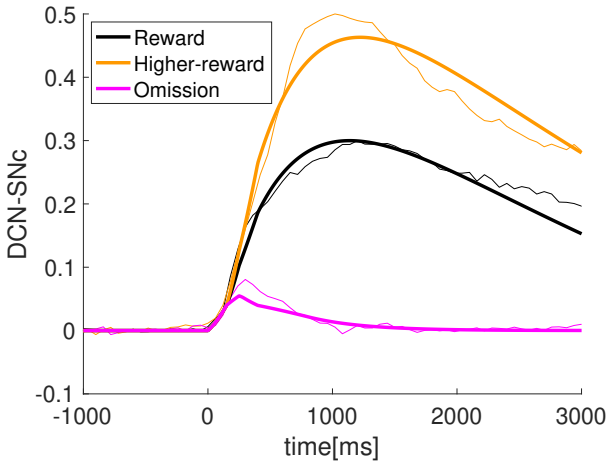


Figure 10: **DCN model output (DCN-SNc estimate).** Thick traces represent the model output for each of the experiments that mice were subject to. Thin traces represent the actual experimental data. It has been rescaled ($\times 1/40$) so that all signals are between 0 and 1, and within the scale of the model output.

We notice that the model does produce an overall good fit and it is able to reproduce the main features of experimental data.

1. Sustained activity after external inputs are applied, for the reward and higher-reward cases.
2. The omission signal decreases immediately after the cue external input terminates.
3. It captures slope differences specially in the first second after the cue when external inputs are applied for the reward and higher reward cases. Between the cue and reward inputs, it is observed a slightly decrease in the slope.

Data shows variability from animal to animal and even from trial to trial. The proposed model produces a similar averaged output. However, it shows a broader range of behaviours. In particular, connectivity parameters can be modified to produce different output shapes. Figure. 11 shows some additional output shapes. This flexibility could be used in order to model single trial data.

## 4.3 Discussion

We have presented a plausible rate-based model, with recurrent excitation and adaptation, modeling the output signal from the DCN to the SNc (DCN-SNc signal).

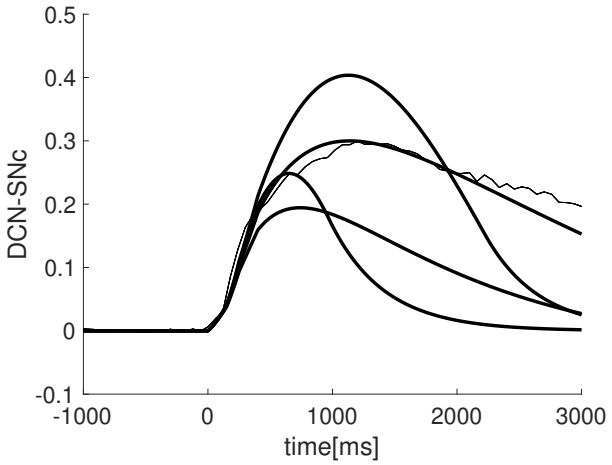


Figure 11: **DCN model additional outputs.** An instance of additional DCN model outputs by modifying connectivity parameters. Reward experiment. The thin trace represent the actual experimental data in the reward case.

The model receives different sensory input signals for each of the trial cases. For all of them a positive cue signal with sort duration is applied at the light time. This signal might represent expectation to the reward. Positive input signals are also associated with reward and higher reward and are applied with some delay and short duration after the light time. However, a negative signal is instead applied to the omission case. This negative signal, which is associated with the lack of reward (or higher-reward) in the omission case, might be modelling disappointment due to the lack of reward.

Overall, the model produces a good fit for each of the three trial cases. From one trial case to another, only input parameters, in particular pulses' heights, are modified and, therefore, intrinsic and connectivity parameters remain fixed.

We have also carried out a phase-plane analysis of the model, and show that external sensorimotor inputs change the phase-plane diagram in such a way that only one stable (active) equilibrium point is present. When external inputs are applied, signals go towards that the active equilibrium, but once they are terminated, signals come back to the rest equilibrium point. We have also briefly discuss that the model is able to reproduce other shapes by changing the connectivity parameters.

In summary, we have proposed a simple model, which is nevertheless complex enough to reproduce experimental data. In the following chapter 5, we will embed this model into a novel neural network model with different basal ganglia interconnected nuclei.

# 5. A feedforward and feedback inhibitory network model

In this chapter, we build a rate-based neuronal network model including the cerebellar-to-SNc pathway. The model includes the following nuclei: the deep cerebellar nuclei (DCN), dopaminergic neurons in the substantia nigra pars compacta (SNc.DA), GABA neurons in the substantia nigra pars compacta (SNc.GABA) and GABA neurons in the substantia nigra pars reticulata (SNr.GABA). It includes feedforward and feedback inhibition between populations [16]. The goal is to propose a plausible network architecture reproducing experimental dopaminergic activity in the SNc.

## 5.1 Methods

The model is a firing rate neural network model in which the activity of each population is described by its firing rate. Four nuclei constitute the neural network model: the DCN ($r_{1e}$), the SNc.GABA ($r_{2i}$), the SNc.DA ($r_{2e}$) and the SNr.GABA ($r_{3i}$). A schematic of the network is shown in Figure. 12.

The model is given by

$$\tau_{1e}\frac{dr_{1e}}{dt} = -r_{1e} + \text{relumax}(J_{1e,1e}r_{1e} - J_{1e,a}a + I_{cue,1e} + I_{rew} + I_{hrew}; m_{1e}, k_{1e}) \tag{8}$$

$$\tau_{a}\frac{da}{dt} = -a + \text{relumax}(J_{a,1e}r_{1e}; m_{a}, k_{a}) \tag{9}$$

$$\tau_{2e}\frac{dr_{2e}}{dt} = -r_{2e} + \text{halfsig}(J_{2e,1e}r_{1e} - J_{2e,2i}r_{2i} + J_{2e,3i}r_{3i} + I_{cue,2e}; m_{2e}, k_{2e}) \tag{10}$$

$$\tau_{2i}\frac{dr_{2i}}{dt} = -r_{2i} + \text{halfsig}(J_{2i,2e}r_{2e}; m_{2i}, k_{2i}) \tag{11}$$

$$\tau_{3i}\frac{dr_{3i}}{dt} = -r_{3i} + \text{halfsig}(J_{3i,1e}r_{1e}; m_{3i}, k_{3i}) \tag{12}$$

Eqs. 8-9 constitute the DCN model described in Chapter 4. Eqs. 10-12 define the rest of the network and model three different neural population within the basal ganglia as described above. We notice that unlike the DCN, we have not included adaptation in the other neuronal populations. Our primary goal is not to build the most accurate network model but to build the simplest network architecture producing a good fit with the data.

The relumax activation function is given by Eq. 6. For the neural population in the basal ganglia a half sigmoid activation function has been used

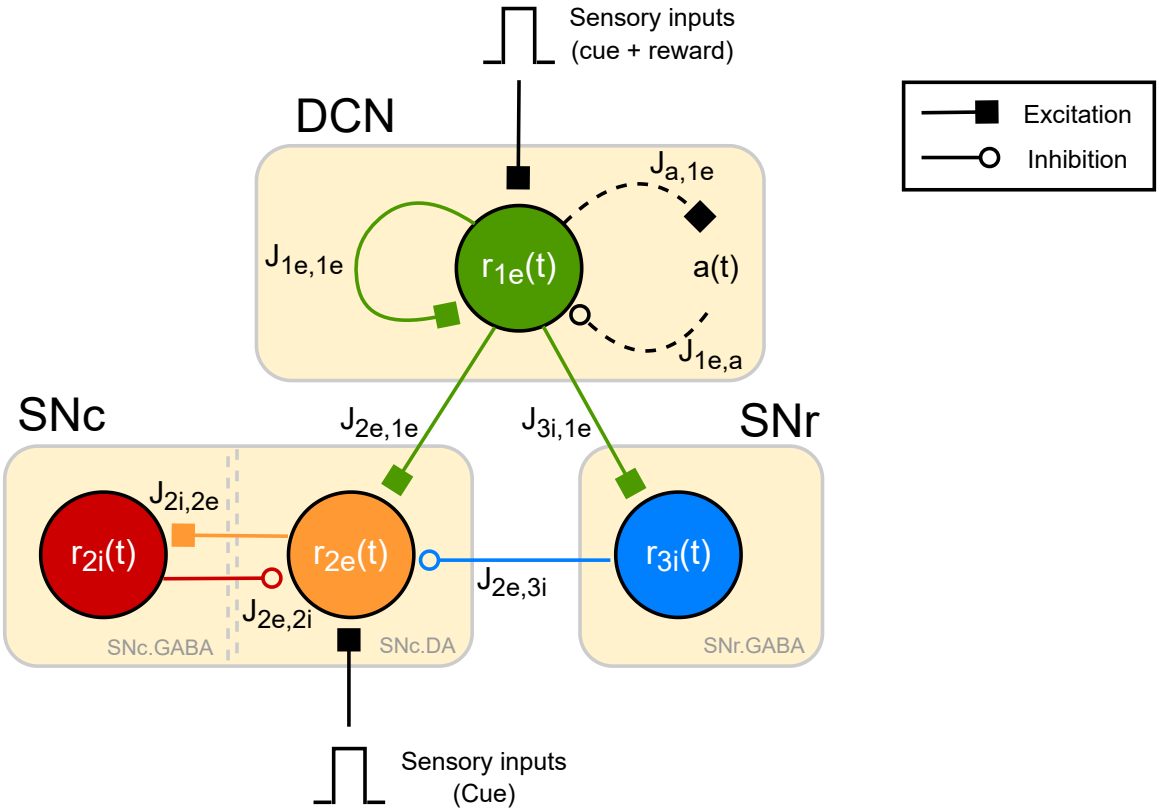


Figure 12: **Neuronal network model schematic.** The models consists of four interconnected neuronal populations: DCN, SNc.DA, SNc.GABA and SNr.GABA. The DCN acts as the input layer projecting to dopaminergic neurons in the SNc (SNc.DA) and GABAergic neurons in the SNr (SNr.GABA). The model also includes recurrent connectivities between neuronal population in the SNc and SNr.

$$\text{halfsig}(I; m, k) = \max\left(0, \frac{2}{1 + e^{-2(I-m)/k}} - 1\right) \tag{13}$$

The choice of a half sigmoid activation function is based on previous model testing and the fact that we were not able to produce a good fit of the data with simpler functions (piece-wise linear approximations).

Sensory inputs, either to the DCN or the SNc.DA neurons are modeled as in Eq. 7. Sensory inputs are injected both to the DCN and the SNc.DA population neurons. However, while both cue and reward (or higher-reward) inputs are applied to the DCN as in Chapter 4, only the cue input, $I_{cue,2e}$, is applied to the SNc.DA neurons. This is a remarkable fact since reward (or higher-reward) information is somehow processed from the DCN to the SNc.DA though the network architecture. We have injected the cue input into the SNc.DA neurons because at the onset of the signal, the SNc.DA activity appears to increase much faster than the DCN activity, see Figure. 3. We remind that the cue input is injected during the first 250 milliseconds after the cue.

We notice that the sub-network formed by the DCN, SNr.GABA and SNc.DA constitute an incoherent feedforward loop inhibition architecture, whereas the one formed by the DCN, SNc.DA and SNc.GABA constitute a feedback inhibitory architecture. We found that both mechanisms are enough in order to reproduce dopaminergic activity in the SNc.

Figure. 12 shows that the DCN is also projecting into SNr.GABA neurons. This is biologically plausible [13], and enables us to include the feedforward inhibitory mechanism.

The model incorporates 17 new parameters to the set of parameters modeling the DCN (Table. 1): 9 intrinsic parameters, 5 connectivity parameters and 3 sensory parameters. They are summarized in Table. (2). Some of them have been chosen based on previous analysis of the model architectures and mechanisms and others have been obtained using a parameter estimation algorithm. See more details in Appendix A.

| Additional network model parameters | | |
|---|---|---|
| Intrinsic | Connectivity | Input |
| $\tau_{2e}$, $\tau_{2i}$, $\tau_{3i}$ | $J_{2e,1e}$, $J_{3i,1e}$ | $J_{cue}$ |
| $m_{2e}$, $m_{2i}$, $m_{3i}$ | $J_{2e,2i}$, $J_{2i,2e}$ | $t_0^{cue}$ |
| $k_{2e}$, $k_{2i}$, $k_{3i}$ | $J_{2e,3i}$ | $t_1^{cue}$ |

Table 2: **Additional network model parameters.** The model has 18 new parameters, apart from the set of parameters defined in the DCN model, Table. 1.

## 5.2 Results

In this section we present the model output. The set of parameter values used, as well as a brief description of how they have been obtained is found in Table. 4. Figure. 13 shows the model output for each nuclei and for each of the three trial cases that mice were subject to.

We have found that both feedforward and feedback inhibition from different neurons is needed in order to reproduce the data. However, we note that the fit is not that accurate for the omission case, specially for large times. The model in not able to reproduce the negative signal presented in the omission case for large times.

The proposed network models incorporates two different mechanisms: feedforward and feedback inhibition producing a pattern of dopaminergic activity in the SNc similar to experimental data. Figure. 14 shows SNc.DA activity int the absence of either feedforward or feedback inhibition. In both cases, the absence of inhibition leads to higher signals, but we have increased the remaining active inhibitory mechanism in order to illustrate how the model would fit the data if only feedback or feedforward inhibition were present.

Figure. 14-(left) shows the effect of feedback inhibition in the absence of feedforward inhibition. We observe that the inhibitory effect is stronger in the first second after the cue, see negative peak in the

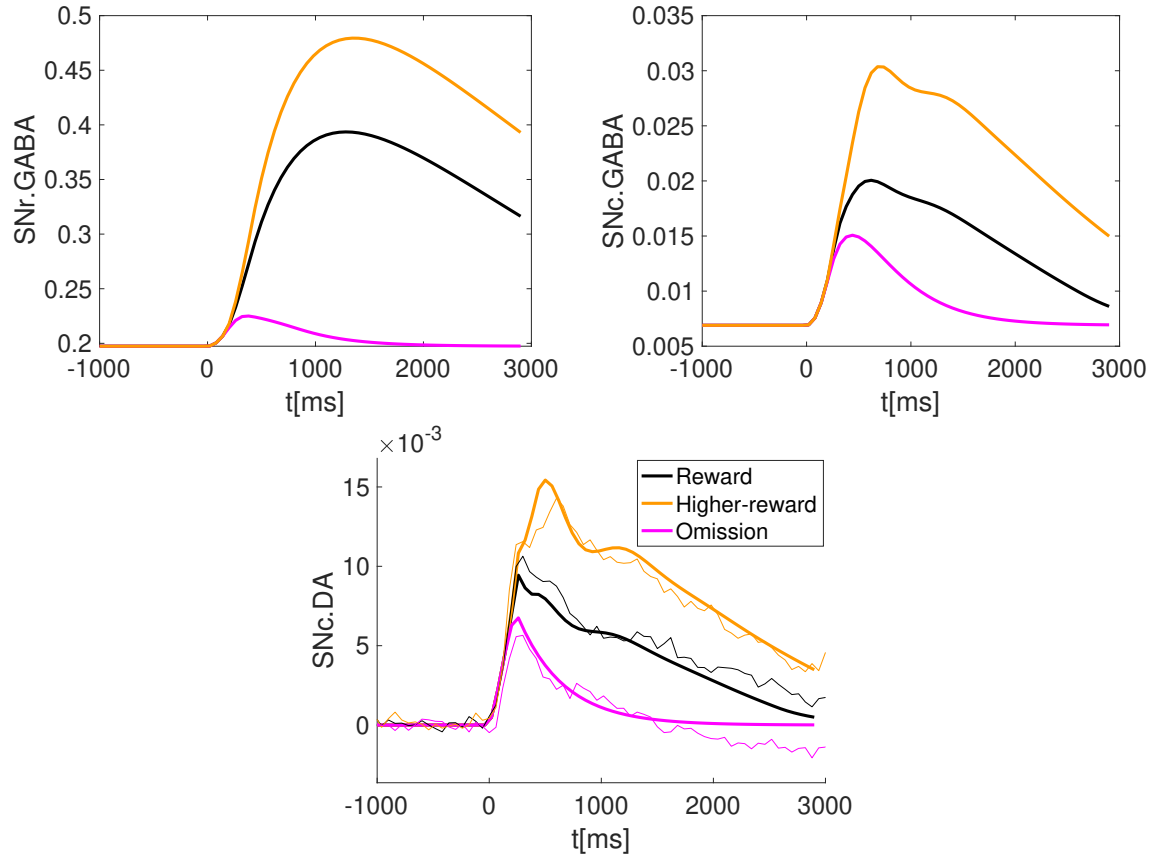


Figure 13: **Network model output.** Top left: SNr.GABA activity. Top right: SNc.GABA activity. Bottom: SNc.DA activity. Thick traces represent the model output for each of the experiments that mice were subject to. Thin traces represent the actual experimental (re-scaled) data.

omission case. On the contrary, Figure. 14-(right) shows the effect of feedforward inhibition in the absence of feedback inhibition. In this case, we see how the inhibitory effect is weaker specially in the first second after the cue, see concave shape in the reward or higher-reward cases.

Regardless the inability of the model to match the negative signal in the omission case, the model does produce an overall good fit and it is able to reproduce the main features of experimental data.

1. Fast increasing slope during the cue input after the cue delivery.

2. Fast decreasing slope for the omission case after the cue, while slower decreasing slopes in the reward and higher reward cases.

3. Increased signal around the higher-reward input for the higher-reward signal, see the peak in the higher-reward signal in the first second after the cue.

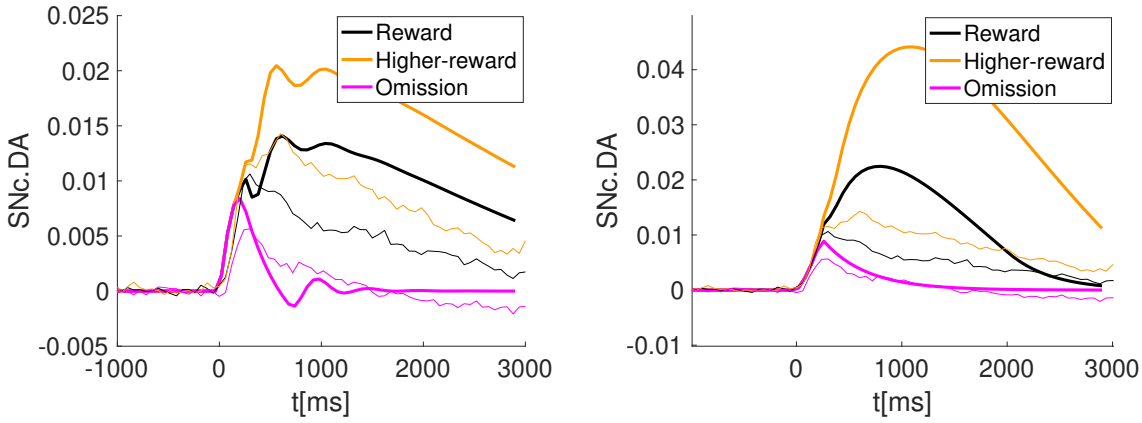


Figure 14: **SNc dopaminergic activity in the absence of either feedforward or feedback inhibition.** Left: Absence of feedforward inhibition. Parameter values: $J_{2e,3i} = 0$ and $J_{2e,2i} = 10.75$; Right: Absence of feedback inhibition. Parameter values: $J_{2e,3i} = 0$ and $J_{2e,2i} = 1.17$

## 5.3 Discussion

We have presented a plausible rate-based neural network model reproducing the main features of experimental data in the SNc.DA neurons. Although the model produces an overall good fit, further research should be done in order to uncover the mechanisms behind the negative signal in the omission case for large times.

Nevertheless, we hypothesize that two different inhibitory mechanisms might play a fundamental role in order to reproduce dopaminergic activity in the SNc: feedforward and feedback inhibition.

# 6. Conclusion

In Chapters 3-5, we have described three modelling tasks. As a first step, we conducted a simple data analysis, consisting in a decoding task. We were able to quantify the different components sent from the cerebellum (DCN) to the dopaminergic neurons in the SNc. Afterwards, we have built a rate-based neuronal network model including the output of the cerebellum (DCN) and three additional populations within the basal ganglia (SNc.DA, SNc.GABA and SNr.GABA). The construction of this neuronal network model was divided into chapters 4 and 5. In Chapter 4, we have first modeled the DCN, which constitutes the input layer to the full network model presented later in Chapter 5. It has been modeled as a neuronal excitatory population model subject to adaptation. In Chapter 5, we have finally described the remaining of the network model and presented the whole network model.

The major outcome of part I is given in Chapter 5. We have been able to propose a novel neuronal network model including two different inhibitory mechanisms that reproduces experimental recordings. We notice that this work is the first one aimed to model the experimental data described in Chapter 2.

## 6.1 Future work

In previous chapters, we have mentioned some lines of future research. In Chapter 3, we suggest that a more robust model could be implemented in order to decode the data. For instance, one could test the hypothesis that there is no cue component, which seems reasonable since the cue and the reward are given simultaneously to mice. Another possibility is to consider that the kernels vary depending on the lick time. That is, different kernels, maybe different shapes, depending on the lick time position.

In Chapter 4 we suggest that our DCN model could be used in order to fit single trial data. Finally, in chapter 5, the major issue to be solved is related with the unknown mechanism that should be producing a negative signal after the cue in the omission case. Our proposed neural network model is not able to reproduce this feature. The goal would be to reproduce this feature, maybe incorporating new connectivities and/or neuronal populations.

# Part II

# Frequency Response of Neurons to Presynaptic Spike Trains

**Summary:**

Variability in neuronal activity is found in experiments across trials, [17]. Although variability in neuronal responses has been exhaustively described, the mechanisms underlying variable responses to fluctuating spike inputs are not well understood [15], [14]. We use simplified feedforward network model with short-term plasticity in order study the response to different presynaptic inputs with different degrees of variability. We show that the input variability does alter the response of postsynaptic cells and characterize the relationship between input and output variabilities.

**Supervised by:** Horacio G. Rotstein and Rodrigo Pena

# 7. An analysis in feedforward networks with short-term plasticity.

## 7.1 Introduction

On the one hand, variability in neuronal activity is found in experiments across trials, [17]. However, the mechanism underlying variable responses to fluctuating spike inputs are not well understood, [15], [14]. Recent work has shown that variable responses might underlay information processing and codification, [5].

On the other hand, short-term plasticity is also thought to play a important role in information processing [4]. It refers to a dynamical synapse phenomenon in which synapse strength changes over times reflecting presynaptic activity. Two opposite phenomenons contribute to the short-term plasticity: short-term depression and short-term facilitation. We refer the reader to [21] for more information about these two mechanisms. The fast time scale of short-term plasticity and the fact that the response of the postsynaptic cell is somehow dependent on the activity of the presynaptic cell links short-term plasticity with information processing.

In this chapter, we consider a simplified feedforward network with sort-term plasticity. It consists of a presynaptic cell modeled as a spike train followed by a passive cell, Figure. 15. Synaptic dynamic is given by the DA (Dayan-Abbot) model for synaptic depression and facilitation. We conduct a systematic study of the steady-state response of the postsynaptic cell when subject to different types of presynaptic inputs with different types of variability:

- Periodic presynaptic inputs with frequency $f_{spk} = 1000/\Delta_{spk}$.
- Poisson-distributed presynaptic inputs with mean rate $r_{spk} = 1000/ < \Delta_{spk} >$, [3].
- Jittered or gaussian perturbations of periodic spike inputs characterized by the jitter variance $\sigma^2$.

We use simulation computational tools to 1. study how the frequency response of the postsynaptic cell changes as presynaptic input changes and 2. characterize how the variability of the response depends on the inputs and the intrinsic cell properties.

## 7.2 Methods

### 7.2.1 Postsynaptic cell

The current-balance equation for the post-synaptic cell is given by

$$C\frac{dV}{dt} = -G_L(V - E_L) + I_{app} - I_{syn} \tag{14}$$

where t is time (ms), V represents the voltage (mV), C is the specific capacitance ($\mu F/cm^2$), $G_L$ is the leak conductance ($mS/cm^2$), $I_{app}$ is the ionic (DC) current ($\mu A/cm^2$) and $I_{syn}$ is an excitatory synaptic current of the form

$$I_{syn} = G_{syn}S(V - E_{syn}) \tag{15}$$

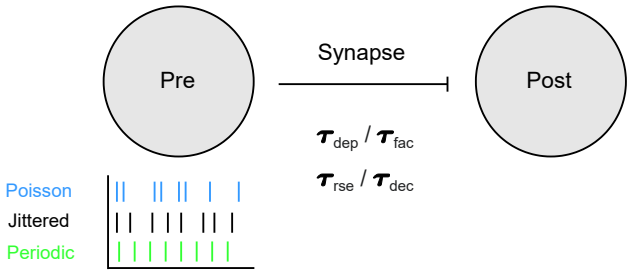


Figure 15: **Feedforward network diagram in the presence of short-term plasticity.** The presynaptic cell is modeled as a spike train either periodic, jittered or Poisson distributed. The postsynaptic cell is modeled as passive cell (capacitive and leak current). The excitatory synaptic function S raises and decays with time constant $\tau_{rse}$ and $\tau_{dec}$, respectively. The synaptic depression and facilitation time constants are $\tau_{dep}$ and $\tau_{fac}$, respectively.

where $G_{syn}$ is the maximal synaptic conductance ($mS/cm^2$), $E_{syn}$ is the reversal potential and $S$ is the synaptic variable.

### 7.2.2 Synaptic dynamics

The synaptic variable $S$ obeys a kinetic equation of the form

$$\frac{dS}{dt} = N(V_{pre})\frac{\Delta S - S}{\tau_r} - \frac{S}{\tau_d} \tag{16}$$

where $V_{pre}$ is the membrane potential of the presynaptic spike, $N(V)$ denotes the sigmoid function

$$N(V) = \frac{1 + \tanh(V/4)}{2} \tag{17}$$

$\tau_{rse}$ and $\tau_{dec}$ are the rise and decay time constants respectively (msec), and $\Delta S$ is a target value for S. In the absence of synaptic dynamics (depression and facilitation), $\Delta S = 1$. Otherwise, $\Delta S$, interpreted as the magnitude $\Delta S$ of the synaptic release per presynaptic spike, is determined as described below.

### 7.2.3 The DA (Dayan-Abbott) model for synaptic depression and facilitation

This phenomenological model is presented in [3]. The magnitude $\Delta S$ of the synaptic release per presynaptic spike is assumed to be the product of the depression (x) and the facilitation (z) variables

$$\Delta S = x^- z^+ \tag{18}$$

where

$$\frac{dx}{dt} = \frac{x_\infty - x}{\tau_{dep}} - a_d x \delta(t - t_{spk}) \tag{19}$$

and

$$\frac{dz}{dt} = \frac{z_\infty - z}{\tau_{fac}} + a_f(1 - z)\delta(t - t_{spk}) \tag{20}$$

Each time a presynaptic spike arrives ($t = t_{spk}$), the depression variable x is decreased by an amount $a_d x$ (the release probability is reduced) and the facilitating variable $z$ is increased by an amount $a_f(1 - z)$ (the

release probability is augmented). During the presynaptic ISIs both $x$ and $z$ decay exponentially to their saturation value $x_\infty$ and $z_\infty$ respectively. The rate at which it occurs is controlled by the parameter $\tau_{dep}$ and $\tau_{fac}$. The superscripts " $\pm$ " in the variables $x$ and $z$ indicate that the update is carried out by taking the values of these variables prior ($^-$) and after ($^+$) the arrival of the presynaptic spike.

### 7.2.4 Presynaptic spike-trains

We model the spiking activity of the presynaptic cell as a spike train with presynaptic spike times

$$t_1, t_2, \dots, t_N \tag{21}$$

We consider three types of input spike-trains: periodic (uniform), Poisson distributed and jittered.

Periodic spike inputs are characterized by the interspike interval (ISI) of length $\Delta_{spk}$ (msec) or, alternatively, by the spiking frequency (Hz)

$$f_{spk} = \frac{1000}{\Delta_{spk}} \tag{22}$$

Poisson distributed spike inputs are characterized by the mean spiking rate (and the associated exponential distribution of ISIs).

Finally, jittered spike inputs correspond to gaussian perturbations of periodic spike inputs. That is, if the spike train for periodic inputs is given by

$$t_{per,1}, t_{per,2}, \dots, t_{per,N} \tag{23}$$

then jittered spike inputs are obtained as

$$t_{per,1} + \delta_1, t_{per,2} + \delta_2, \dots, t_{per,N} + \delta_N \tag{24}$$

where $\{\delta_i\}_{i=1}^N$ are normally distributed with zero mean and variance $\sigma^2$.

Figure. 16 illustrates voltage traces for periodic spike inputs (left) and for a non-uniform spike train, poisson-distributed (right). For each presynaptic spike there is a maximum and a minimum in voltage traces, marked as red and green circles respectively.

We characterize the frequency response by its amplitude and peak profile. For each presynaptic spike, its associated amplitude in the voltage response is defined as the difference between it associated maximum and minimum in the voltage trace. The peak corresponds to the associated maximum. For non-periodic spike inputs, the presynaptic input spike train produces a distribution of amplitudes and peaks in the response. For periodic spike inputs, in steady state, the amplitude and peak profiles are constant.

## 7.3 Implementation

The numerical solutions were computed using the modified Euler method (Runge-Kutta, order 2) with a time step t = 0.01 ms (or smaller values of t when necessary) in MATLAB (The Mathworks, Natick, MA). The code is available at `https://github.com/guillermovillanuevabenito/TFM`.

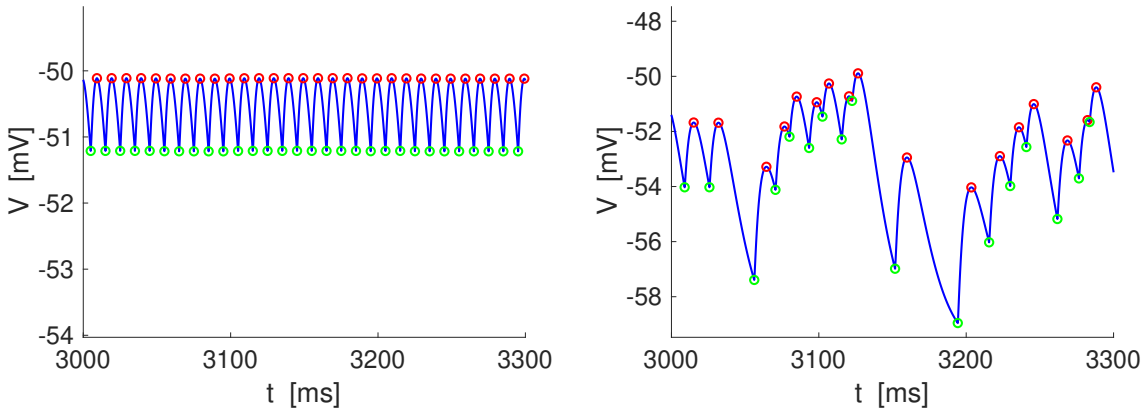


Figure 16: **Voltage traces of postsynaptic cell.** Left: periodic spike inputs.; Right: poisson-distributed spike inputs. Maxima and minima in voltage traces are marked as red and green circles respectively. Parameter values: $C = 1$, $G_L = 0.1$, $E_L = -60$, $I_{app} = 0$, $G_{syn} = 0.1$, $E_{syn} = 0$, $\tau_r = 0.1$, $\tau_d = 10$, $x_\infty = 1$, $z_\infty = 0$, $a_d = 0.1$, $a_f = 0.1$, $\tau_{fac} = 100$, $\tau_{dep} = 100$, input frequency (rate) $= 100Hz$.

## 7.4 Results

Figure. 17 shows the frequency response for the three different spike inputs. The top panel shows it for small values of both depression and facilitation time constants while the bottom panel shows it for larger values of both depression and facilitation time constants. Notice how even small jitter ($\sigma = 0.25\Delta_{spk}$) produces a slightly different frequency response with respect to the periodic input response.

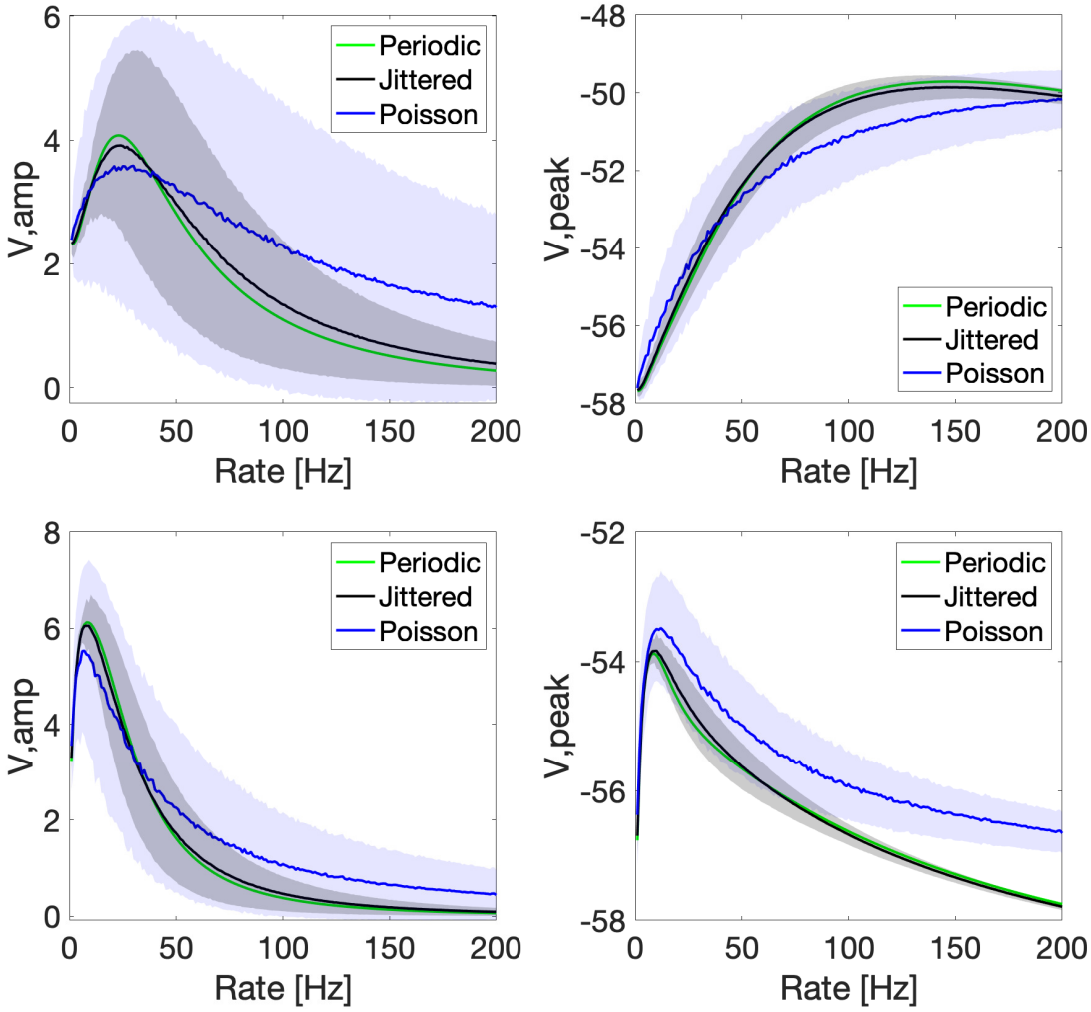


Figure 17: **Frequency response of postsynaptic cell.** Left: Voltage amplitude profile; Right: Voltage peak profile. Lines represent the mean profile, while shadowed areas represent the one standard deviation interval. Three presynaptic spike inputs: periodic, jittered and poisson-distributed; Top: $\tau_{fac} = 100$, $\tau_{dep} = 100$; Bottom: $\tau_{fac} = 1000$, $\tau_{dep} = 1000$. Remaining parameter values: $C = 1$, $G_L = 0.1$, $E_L = -60$, $I_{app} = 0$, $G_{syn} = 0.1$, $E_{syn} = 0$, $\tau_r = 0.1$, $\tau_d = 10$, $x_\infty = 1$, $z_\infty = 0$, $a_d = 0.1$, $a_f = 0.1$, $\sigma = 1/4\Delta_{spk}$.

**Statement 7.1.** *The mean amplitude and peak profiles for non-periodic presynaptic spike inputs do not coincide with the periodic spike input profiles.*

Figure. 17 also show the one standard deviation interval as a shadowed area. For both the amplitude and the peak profiles, there is a frequency for which their variance reaches its maximum.

**Statement 7.2.** *The amplitude and peak profiles of the response to non-periodic spike inputs show a frequency for which the their variance reaches its maximum.*

The change of depression and facilitation time constants does change the maximum variance frequency in the amplitude profile, i.e., the frequency associated with maximum variance, Figure. 18.

**Statement 7.3.** *An increase in both depression and facilitation time constants leads to a decrease in the frequency associated with the maximum variance in the amplitude profile. Moreover, jittered spike inputs with higher variance produce a higher decrease.*

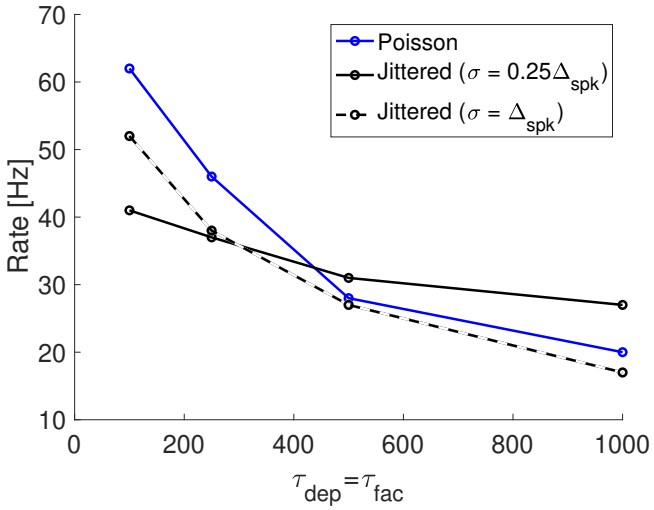


Figure 18: **Decrease in the maximum variance frequency in the amplitude profile as a functions of depression and facilitation time constants.** Parameter values: $C = 1$, $G_L = 0.1$, $E_L = -60$, $I_{app} = 0$, $G_{syn} = 0.1$, $E_{syn} = 0$, $\tau_r = 0.1$, $\tau_d = 10$, $x_\infty = 1$, $z_\infty = 0$, $a_d = 0.1$, $a_f = 0.1$, $\sigma = 1/4\Delta_{spk}$.

Figure. 19 shows the effect on the response of an increase in the input variance for jittered spike inputs. We observe that higher input variance leads to an overall increase in the output variance for both the amplitude and peak profiles. We ask which is the dependence between the input variance and the output variance in the profiles.

In order to answer the above question, we consider jittered spike inputs with different degrees of variance. Figure. 20 shows the variability in the amplitude (left) and peak (right) profiles as a function of the normalized standard deviation ($\sigma/\Delta_{spk}$). The black line represents the mean of the variance while shadowed areas represent the one standard deviation interval.

**Statement 7.4.** *An increase in the input variance for jittered spike inputs produces a higher variability in the amplitude and peak profiles of the voltage response. Moreover, the rate of increase is higher in the smaller variance regime.*

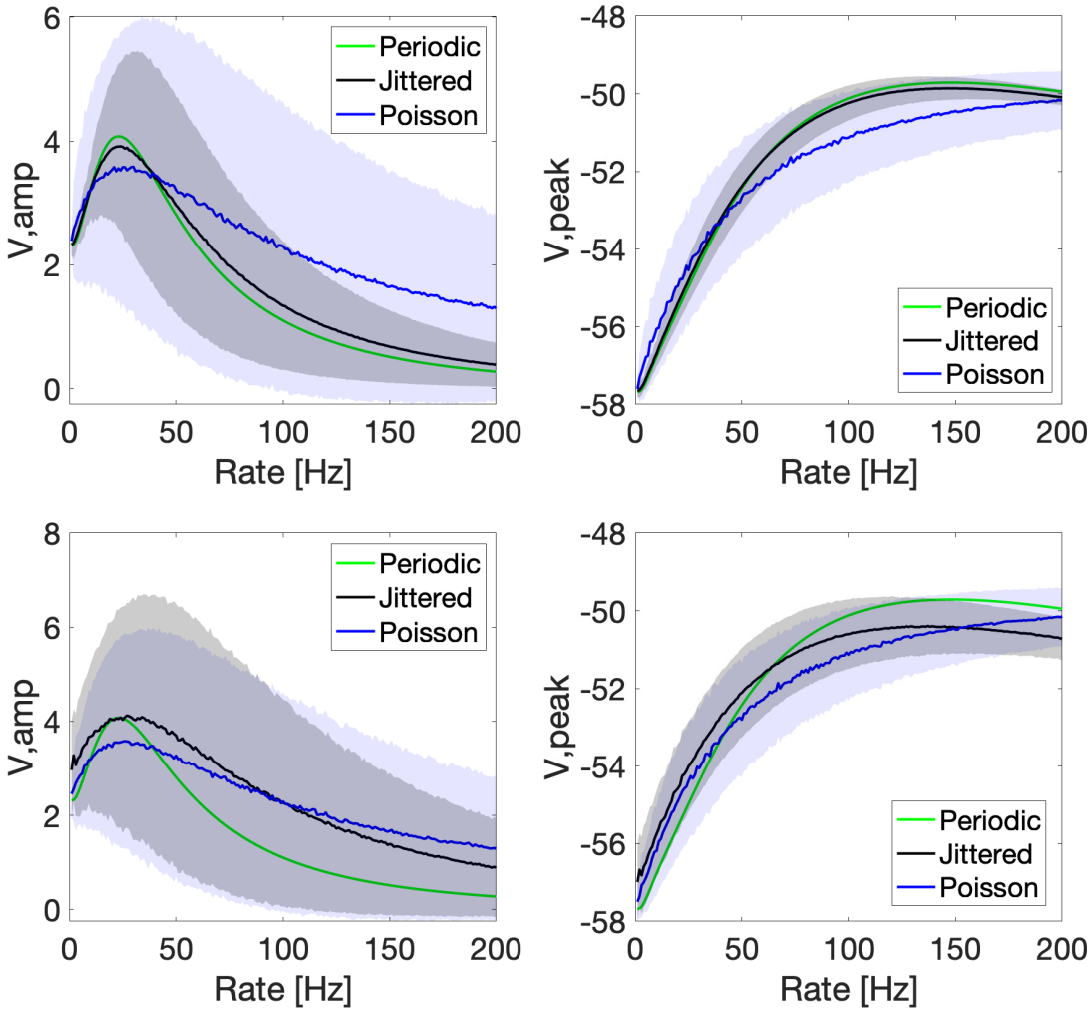


Figure 19: **Increase in the output variance as the input variance (jittered spike inputs) increases**. Left: Voltage amplitude profile; Right: Voltage peak profile. Lines represent the mean profile, while shadowed areas represent the one standard deviation interval. Three presynaptic spike inputs: periodic, jittered and poisson-distributed; Top: Parameter values: $\sigma = 1/4\Delta_{spk}$; Bottom: Parameter values: $\sigma = 5/4\Delta_{spk}$. Remaining parameter values: $C = 1$, $G_L = 0.1$, $E_L = -60$, $I_{app} = 0$, $G_{syn} = 0.1$, $E_{syn} = 0$, $\tau_r = 0.1$, $\tau_d = 10$, $x_\infty = 1$, $z_\infty = 0$, $a_d = 0.1$, $a_f = 0.1$, $\tau_{fac} = 100$, $\tau_{dep} = 100$.

## 7.5 Conclusion and future work

In this chapter, we have analyzed the frequency response in a feedforward network model with short-term plasticity and provided a set of results linking the variability in the response with the input variability. We have shown that the frequency response changes with the input variability and that a systematic increase in the input variability leads to more variable responses. We characterize frequency responses with their respective amplitude and peak profiles.

Our work is summarized in a set of four statements which constitute a first attempt to characterize neuronal

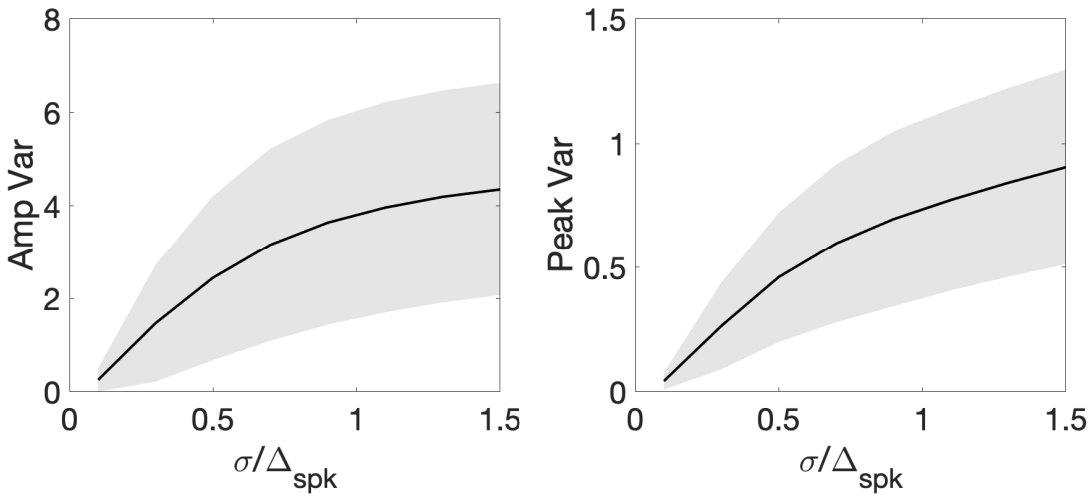


Figure 20: **Variability in the response as a function of the input variability (jittered spike inputs).** Left: Variability in the voltage amplitude profile; Right: Variability in the voltage peak profiles. Lines represent the mean variance, while shadowed areas represent the one standard deviation interval. Parameter values: $C = 1$, $G_L = 0.1$, $E_L = -60$, $I_{app} = 0$, $G_{syn} = 0.1$, $E_{syn} = 0$, $\tau_r = 0.1$, $\tau_d = 10$, $x_\infty = 1$, $z_\infty = 0$, $a_d = 0.1$, $a_f = 0.1$, $\tau_{fac} = 100$, $\tau_{dep} = 100$.

variability in a simplified network model. We provide the code developed for this chapter for future studies. More work should be done in order to fully characterized the variability in the response. In particular different sets of intrinsic and synaptic parameters can be used in order to study its their effect on the response.

# References


[1] Bostan AC and Strick PL. The basal ganglia and the cerebellum: nodes in an integrated network. *Nat Rev Neurosci*, 2018.

[2] Fabio Blandini, Giuseppe Nappi, Cristina Tassorelli, and Emilia Martignoni. Functional changes of the basal ganglia circuitry in parkinson's disease. *Progress in Neurobiology*, 62(1):63–88, 2000.

[3] Peter Dayan and L. F. Abbott. *Theoretical Neuroscience: Computational and Mathematical Modeling of Neural Systems*. The MIT Press, 2001.

[4] Pan-Yue Deng and Vitaly A. Klyachko. The diverse functions of short-term plasticity components in synaptic computations. *Communicative & Integrative Biology*, 4(5):543–548, 2011. PMID: 22046457.

[5] Mingzhou Ding, PhD and Dennis Glanzman, PhD. *The Dynamic Brain: An Exploration of Neuronal Variability and Its Functional Significance*. Oxford University Press, 01 2011.

[6] G.B. Ermentrout and D. Terman. *Mathematical Foundations of Neuroscience*. Springer, New York, 2010.

[7] Medina JF. Teaching the cerebellum about reward. *Nat Neurosci*, 2019.

[8] Raymond JL and Medina JF. Computational principles of supervised learning in the cerebellum. *Annu Rev Neurosci*, 2018.

[9] Leila Khatami Jorge Vera Farzan Nadim Kamran Khodakhah Junichi Yoshida, Maritza Oñate. Cerebellar contributions to the basal ganglia influence motor coordination, reward processing and movement vigor. 2022.

[10] Bhatia KP and Marsden CD. The behavioural and motor consequences of focal lesions of the basal ganglia in man. *Brain*, 1994.

[11] José Lanciego, Natasha Luquin, and José Obeso. Functional neuroanatomy of the basal ganglia. *Cold Spring Harbor perspectives in medicine*, 2, 10 2012.

[12] Jung MW.s Lee D, Seo H. Neural basis of reinforcement learning and decision making. *Annu Rev Neurosci.*, 2012.

[13] Laurie Lundy-Ekman. *Neuroscience*. 04 20022.

[14] Yugarshi Mondal, Rodrigo F. O. Pena, and Horacio G. Rotstein. Temporal filters in response to presynaptic spike trains: Interplay of cellular, synaptic and short-term plasticity time scales. *bioRxiv*, 2022.

[15] Rodrigo F. O. Pena and Horacio G. Rotstein. Oscillations and variability in neuronal systems: interplay of autonomous transient dynamics and fast deterministic fluctuations. *bioRxiv*, 2021.

[16] Michiel W.H. Remme and Wytse J. Wadman. Control of a local neural network by feedforward and feedback inhibition. *Neurocomputing*, 58-60:683–689, 2004. Computational Neuroscience: Trends in Research 2004.

[17] Alfonso Renart and Christian K Machens. Variability in neural activity and behavior. *Current Opinion in Neurobiology*, 25:211–220, 2014. Theoretical and computational neuroscience.

[18] Hernán I. Savastano and Ralph R. Miller. Time as content in pavlovian conditioning. *Behavioural Processes*, 44(2):147–162, 1998.

[19] David Sterratt, Bruce Graham, Andrew Gillies, and David Willshaw. *Principles of Computational Modelling in Neuroscience*. Cambridge University Press, 2011.

[20] Steven H. Strogatz. *Nonlinear Dynamics and Chaos: With Applications to Physics, Biology, Chemistry and Engineering*. Westview Press, 2000.

[21] M. Tsodyks and S. Wu. Short-term synaptic plasticity. *Scholarpedia*, 8(10):3153, 2013. revision #182521.

[22] Maia TV and Frank MJ. From reinforcement learning models to psychiatric and neurological disorders. *Nat Neurosci*, 2011.

[23] Samantha Washburn, Maritza Oñate, Junichi Yoshida, Jorge Vera, Ramakrishnan K. B., Leila Khatami, Farzan Nadim, and Kamran Khodakhah. Cerebellum directly modulates the substantia nigra dopaminergic activity. *bioRxiv*, 2022.

# A. Implementation

Code written in MATLAB was used to load and analyze experimental data, estimate the model parameters, simulate the model and generate the figures. The code in hosted in the following GitHub repository: `https://github.com/guillermovillanuevabenito/TFM`. The accompanied "README" file includes detailed information of the algorithms and simulations done.

## DCN model

| Parameter | Value | Description |
|---|---|---|
| $\tau_{1e}$ | 433 | Fit to experimental data |
| $\tau_a$ | 108 | Fit to experimental data |
| $m_{1e}$ | 0.484 | Fit to experimental data |
| $m_a$ | 0.293 | Fit to experimental data |
| $k_{1e}$ | 0.243 | Fit to experimental data |
| $k_a$ | 0.147 | Fit to experimental data |
| $J_{1e,1e}$ | 4 | Fit to experimental data |
| $J_{1e,a}$ | 1.8 | Fit to experimental data |
| $J_{a,1e}$ | 1 | Fit to experimental data |
| $J_{cue}$ | 0.08 | Input parameter |
| $J_{rew}$ | 0.08 | Post tuned |
| $J_{hrew}$ | 0.15 | Post tuned |
| $t_0^{cue}$ | 0 | Based on experimental observations |
| $t_0^{rew}$ | 150 | Based on experimental observations |
| $t_0^{hrew}$ | 150 | Based on experimental observations |
| $t_1^{cue}$ | 250 | Based on experimental observations |
| $t_1^{rew}$ | 400 | Based on experimental observations |
| $t_1^{hrew}$ | 400 | Based on experimental observations |

Table 3: **Parameter values used in the neuronal model presented in Chapter 4.**

## Neuronal network model

| Parameter | Value | Description |
|---|---|---|
| $\tau_{2e}$ | 410 | Fit to experimental data |
| $\tau_{2i}$ | 220 | Fit to experimental data |
| $\tau_{3i}$ | 120 | Fit to experimental data |
| $m_{2e}$ | -0.2 | Fit to experimental data |
| $m_{2i}$ | -0.01 | Fit to experimental data |
| $m_{3i}$ | -0.06 | Fit to experimental data |
| $k_{2e}$ | 1.4 | Fit to experimental data |
| $k_{2i}$ | 1.45 | Fit to experimental data |
| $k_{3i}$ | 0.3 | Fit to experimental data |
| $J_{2e,1e}$ | 0.89 | Fit based on model analysis |
| $J_{3i,1e}$ | 0.21 | Fit based on model analysis |
| $J_{2e,2i}$ | 4.3 | Fit based on model analysis |
| $J_{2i,2e}$ | 2.7 | Fit based on model analysis |
| $J_{2e,3i}$ | 1 | Fit based on model analysis |
| $t_0^{cue,2e}$ | 0 | Based on experimental observations |
| $t_1^{cue,2e}$ | 250 | Based on experimental observations |
| $J_{cue,2e}$ | 0.04 | Input parameter |

Table 4: **Additional set of parameter values used in the neuronal network model presented in Chapter 5**.

# B. Phase plane analysis

The phase plane analysis for Eqs. 4-5 can be solved analytically.

On the one hand, the a-nullcline is directly obtained from the equality,

$$a = \text{relumax}(R_{21} r_{1e}) \tag{25}$$

It is a piece-wise linear function defined as

$$a = \begin{cases} 0 & \text{if } r_{1e} \leq m_a - 2k_a \\ 1/2 + (J_{a,1e} r_{1e} - m_a)/4k_a & \text{if } m_a - 2k_a \leq r_{1e} \leq 2k_a + m_a \\ 1 & \text{if } r_{1e} \geq 2k_a + m_a \end{cases} \tag{26}$$

On the other hand, the $r_{1e}-$nullcline is derived from the equality

$$r_{1e} = \text{relumax}(R_{1e,1e} r_{1e} J_{1e,a} a + I) \tag{27}$$

Doing some manipulations one arrives to the following expression.

If $(m_{1e} - I - 2k_{1e})/J_{1e,a} \leq a \leq (2k_{1e} + m_{1e} - I - J_{1e,1e})/J_{1e,a}$ then

$$r_{1e} = aJ_{1e,a}/(4k_{1e} - J_{1e,1e}) + (2k_{1e} - m_{1e} + I)/(4k_{1e} - J_{1e,1e}) \tag{28}$$

Moreover, if $a \geq (m_{1e} - I - 2k_{1e})/J_{1e,a}$ then

$$r_{1e} = 0 \tag{29}$$

and if $a \leq (2k_{1e} + m_{1e} - I - J_{1e,1e})/J_{1e,a}$ then

$$r_{1e} = 1 \tag{30}$$